Preprint typeset in JHEP style - HYPER VERSION

LU-TP 05-10
hep-ph/0503181

arXiv:hep-ph/0503181 v2 14 Jun 2005

Energy Conservation and Saturation in Small-x Evolution

Emil Avsar, Gösta Gustafson and Leif Lönnblad

Dept. of Theoretical Physics, Sölvegatan 14A, S-223 62 Lund, Sweden
E-mail: Emil.Avsar@thep.lu.se, Gosta.Gustafson@thep.lu.se *and*
Leif.Lonnblad@thep.lu.se

Abstract: Important corrections to BFKL evolution are obtained from non-leading contributions and from non-linear effects due to unitarisation or saturation. It has been difficult to estimate the relative importance of these effects, as NLO effects are most easily accounted for in momentum space while unitarisation and saturation are easier in transverse coordinate space. An essential component of the NLO contributions is due to energy conservation effects, and in this paper we present a model for implementing such effects together with saturation in Mueller's dipole evolution formalism. We find that energy conservation severely dampens the small-x rise of the gluon density and, as a consequence, the onset of saturation is delayed. Using a simple model for the proton we obtain a reasonable qualitative description of the x-dependence of F_2 at low Q^2 as measured at HERA even without saturation effects. We also give qualitative descriptions of the energy dependence of the cross section for $\gamma^\star\gamma^\star$ and $\gamma^\star-$nucleus scattering.

Keywords: QCD, Jets, Parton Model, Phenomenological Models.

Contents

1. Introduction **1**

2. Dipole Cascades in Momentum Space **5**
- 2.1 Time-like Cascades 5
- 2.2 Space-like Cascades 6

3. Dipole Cascades in Coordinate Space **7**
- 3.1 The Mueller Dipole Formulation 7
- 3.2 Unitarity and Saturation 9

4. Combining Energy-Momentum Conservation and Unitarity **10**
- 4.1 Relation Mueller's Dipole Cascade vs. LDC 10
- 4.2 Energy-Momentum Conservation 12
- 4.3 Final States and Virtual Dipoles 13
- 4.4 Gluon Recombination and Frame Dependence 14

5. The Monte Carlo Implementation **16**
- 5.1 Kinematics 16

6. Results **18**
- 6.1 Dipole Multiplicity 18
- 6.2 Onium–Onium scattering. 20
- 6.3 Dipole–nucleus scattering. 22
- 6.4 F_2 at HERA 24

7. Conclusions **26**

1. Introduction

In the asymptotical high-energy limit, QCD should be described by BFKL [1,2] evolution, at least to leading order and assuming a fixed coupling. Here terms of the form $(\alpha_s \log x)^n$ in a perturbative expansion are resummed to all orders. The result is a fast rise of any cross section with increasing energy or, equivalently, with decreasing x. The rise has the form $x^{-\lambda}$, where the power λ to leading order is given by $\bar{\alpha}\, 4 \log 2$, which is around one half for $\bar{\alpha} \equiv 3\alpha_s/\pi = 0.2$. Clearly such a behavior will violate the unitarity bound for large enough energies. To cure this problem Gribov, Levin and Ryskin [3] in pioneering works discussed non-linear effects from gluon recombination, which cause the gluon density to saturate before it becomes too high.

Because the transverse coordinates are unchanged in a high energy collision, unitarity constraints are generally more easy to take into account in a formalism based on the transverse coordinate space representation, and several suggestions for how to include saturation effects in such a formalism have been proposed. Golec–Biernat and Wüsthoff [4] formulated a dipole model, in which a virtual photon is treated as a $q\bar{q}$ or $q\bar{q}g$ system impinging on a proton, and this approach has been further developed by several authors (see e.g. [5] and [6]). Mueller [7–9] has formulated a dipole cascade model in transverse coordinate space, which reproduces the BFKL equation, and in which it is also possible to account for multiple sub-collisions. Within this formalism Balitsky and Kovchegov [10, 11] have derived a non-linear evolution equation, which also takes into account these saturation effects from multi-pomeron exchange. In an alternative approach a high density gluonic system is described by a so-called Color Glass Condensate [12, 13], where non-perturbative effects appear due to the high density, even though the coupling α_s is small.

There are, however, other effects which may dampen the growth of the structure function. One is the fact that the next-to-leading logarithmic corrections to the BFKL evolution turn out to be very large [14, 15]. These corrections strongly suppress the growth for small x, and in fact, even for moderate values of $\bar{\alpha}$, the power λ becomes negative. It is well-known [16] that a major fraction of these higher order corrections is related to energy conservation. The large effect of energy-momentum conservation is also clearly demonstrated by the numerical analyses by Andersen–Stirling [17] and Orr–Stirling [18].

As a consequence there is currently some controversy over whether saturation has been observed in deeply inelastic scattering at HERA. Saturation effects have been studied in the coordinate space representation in which it has been difficult to include non-leading effects, and the non-leading effects have been studied in momentum space, where it is hard to include saturation. Therefore it has been difficult to estimate the relative importance of saturation and non-leading effects. To know if the dominant mechanism behind the reduced growth rate is due to energy conservation or to saturation is also very important for reliable extrapolations to higher energies at LHC and high energy cosmic ray events. Our aim in this paper is to find a formalism where it is possible to account for both unitarisation and energy-momentum conservation, knowing that the latter is a major part of the non-leading effects. An alternative approach to this problem is presented in [19, 20], in which a formalism to include saturation and conservation of energy (or rather the positive lightcone momentum component, p_+) is described. In our formalism we emphasize conservation of both lightcone components, p_+ and p_-.

We emphasize that the question concerning saturation is not whether it exists in general — clearly if the scale is small enough so that the transverse size of the gluons is as big as a nucleon there must be recombinations present — rather the debate is about whether effects of recombination of *perturbative* gluons at scales above a couple of GeV has been observed. The deviation from the linear BFKL evolution, as a consequence of saturation, is expected to be essential below a line $Q^2 = Q_s^2(x)$ in a (Q^2, x) diagram [4]. The effect can be viewed in two different ways, as a suppression of the logarithmic x-slope of the structure function, $d \log F_2 / d \log x \equiv \lambda_{\text{eff}}$, when x becomes small for fixed Q^2, or as a suppression when Q^2 becomes small for fixed x. HERA data show an almost linear dependence of λ_{eff}

with $\log Q^2$, leveling off at ≈ 0.1 for Q^2 below 1 GeV^2, with the proviso that the x-interval used to determine the slope is not constant, but is shifted towards smaller x for smaller Q^2-values (see e.g. refs. [21,22]). The suppression for small x and for small Q^2 also appears to satisfy a scaling property called geometric scaling, saying that F_2 is a function of a single variable $\tau = Q^2/Q_s^2(x)$. This scaling is satisfied by the HERA data to a high degree, and in an early study Golec–Biernat and Wüsthoff found a good fit to experiments with $Q_s^2(x) = (3.04 \cdot 10^{-4}/x)^{0.288}\,\mathrm{GeV}^2$ [4]. In a more recent analysis Iancu, Itakura, and Munier [23] obtained a good fit to later HERA data with a model based on BFKL evolution including some non-leading effects[1] plus saturation, with $Q_s^2(x) = (0.267 \cdot 10^{-4}/x)^{0.253}\,\mathrm{GeV}^2$. This value is smaller than the one in ref. [4], and therefore moves the saturation region closer to the non-perturbative regime.

The Mueller dipole evolution is formulated in rapidity ($\propto \log 1/x$) and transverse coordinate space, with rapidity acting as the evolution parameter. A DIS $\gamma^\star p$ scattering is typically viewed in the rest system of the proton, where the $\gamma^\star$ evolves into a $\mathrm{q\bar{q}}$ pair, long before the interaction. This $\mathrm{q\bar{q}}$ pair will then radiate off gluons, $\mathrm{q\bar{q}} \to \mathrm{qg\bar{q}} \to \mathrm{qgg\bar{q}} \to \ldots$, a process which is formulated in terms of radiation from colour-dipoles. The initial dipole between the q and $\bar{\mathrm{q}}$ emits a gluon, splitting the dipole into two, one between the q and g and one between the g and $\bar{\mathrm{q}}$, both of which can continue radiating gluons. In the end, one of these dipoles can interact with the proton, giving a cross section which increases as a power of $1/x$, and in leading order reproduces the BFKL result. Saturation comes in because when the density of dipoles becomes large there is a possibility that more than one of them interacts with the proton, thus slowing down the increase of the cross section. This effect can be interpreted as multi-pomeron exchange, and is taken into account in the non-linear BK equation.

The Mueller dipole evolution is very similar in spirit to the Dipole Cascade Model (DCM) [25,26], which describes time-like evolution of dipoles from e.g. an initial $\mathrm{q\bar{q}}$ pair created in $\mathrm{e^+e^-}$-annihilation. However, here the evolution is formulated in momentum space. The transverse momentum is used as evolution parameter, and the conservation of energy and momentum is simple to implement, especially in a Monte Carlo Event Generator. This model gives a very good description of $\mathrm{e^+e^-}$ annihilation and the ARIADNE program [27], where it is implemented, describes almost all data from the four LEP collaborations to an astonishing precision (see e.g. [28]). Also with the so-called soft-radiation extension of the DCM, DIS final states as measured by HERA are well described using a simple semi-classical description of time-like dipole evolution (see e.g. [29]).

One problem in Mueller's formulation is the fact that, while the emission probability for a time-like cascade in the DCM is finite for a fixed value of the evolution parameter, the emission probability here diverges $\sim 1/r^2$ for very small dipole sizes r. However, the interactions from the colour charge and anti-charge interfere destructively, resulting in colour transparency, and for small r-values the dipole cross section is proportional to r^2,

[1] Basically, non-leading effects are taken into account by simply lowering the BFKL λ, or treating it as a free parameter, in which case it comes out close to the value predicted by the so-called renormalization-group improved [24] NLO BFKL. Also some non-leading effects are introduced by letting α_s run, typically with Q_s^2 as the scale.

implying that the total cross section remains finite, and the Mueller dipole formulation can be shown to be equivalent to BFKL. Although $\sigma_{\rm tot}$ is finite, the singularities do cause problems. For a numerical analysis or a MC simulation it is necessary to introduce a cutoff for small dipoles, and for small cutoff values the number of dipoles becomes very large. In fact, the increase is so strong that a Monte Carlo simulation of the evolution, as is done e.g. in the OEDIPUS program [30–32], becomes extremely inefficient. It also implies that it is not possible to interpret the dipole chain as a real final state. If a small size in coordinate space corresponds to a large transverse momentum, the very large and diverging number of dipoles with very small sizes obviously violates energy-momentum conservation. Instead these emissions have to be regarded as virtual fluctuations, which in Mueller's approach are handled by appropriate Sudakov form factors.

An alternative approach to DIS is the so-called Linked Dipole Chain (LDC) [33,34] model, where an initial set of gluons is obtained using space-like parton evolution, and then is evolved in time-like cascades into final-state gluons. LDC is a reformulation and generalization of CCFM evolution [35,36], which reproduces BFKL in the asymptotic small-x limit but is also similar to DGLAP evolution [37–40] at larger x values. In addition to sequences of DGLAP evolution, where the *upward* gluon branchings with $k_{\perp i} \gg k_{\perp i-1}$ are strongly ordered in rapidity and in the $k_\perp$ of the propagating gluon, also *downward* splittings with $k_{\perp i} \ll k_{\perp i-1}$ may appear with a reduced weight. The result is an evolution which is totally symmetric, in the sense that it can be generated either from the projectile or from the target end with the same result. The LDC model is completely formulated in momentum space which makes it easy to implement in a Monte Carlo event generator [41], where energy and momentum conservation is easily accomplished.

In this paper we will identify some similarities between the LDC model and the Mueller dipoles, and use them to derive a scheme for implementing energy momentum conservation in the space-like dipole evolution. We conjecture that only gluon emissions which satisfy energy-momentum conservation can correspond to real final state gluons, and that keeping only these (with a corresponding modification of the Sudakov form factor) will not only give a better description of the final states, but also account for essential parts of the NLO corrections to the BFKL equation. Our approach is based on the observation that the emission of a dipole with a very small transverse size, r, corresponds to having two very well localized gluons, and such gluons must have large transverse momenta, of the order of $p_\perp \sim 1/r$. By in this way assigning a transverse momentum to each emitted gluon, and also taking into account the recoils of the emitting gluons, we can then make sure that each dipole splitting is kinematically allowed. However, as will be discussed in detail in section 4.3, energy-momentum conservation is a *necessary* condition for a chain to correspond to a real final state, but it is not a *sufficient* condition. Therefore we will in this paper only discuss results for total cross sections, and postpone discussions of final state properties to a future publication.

The program described here is, of course, not easy to implement in an analytic formalism. Instead we have written a Monte Carlo program, similar to OEDIPUS, where the kinematics can be easily treated. This program can then be used to calculate cross sections for e.g. dipole–dipole scattering at different virtualities. We also introduce a simple model

for nucleons as a distribution in dipole numbers and sizes, to investigate cross sections for dipole–A scattering. In principle this can also be used to study AA scattering, but such investigations will also be postponed for a future publication.

The layout of this paper is as follows. First we describe the dipole cascades formulated both in transverse momentum and in coordinate space in sections 2 and 3. In section 4 we then describe the similarity between the LDC model and Mueller's cascade model, and how this guides us in the introduction of energy-momentum conservation into the Mueller dipole formalism. In this section we also discuss some open questions related to final state properties and gluon recombination. In section 5 we describe briefly the implementation in a Monte Carlo program we use to obtain the results presented in the following section 6. Finally we arrive at our conclusions in section 7.

2. Dipole Cascades in Momentum Space

The Dipole Cascade Model (DCM [25, 26]) as implemented in the ARIADNE [27] event generator has been very successful in describing the bulk of the data on hadronic final states recorded at LEP. In this section we will first describe briefly this model and then go on to how it can be extended to also describe cross sections and hadronic final states in DIS by a reformulation of the CCFM evolution.

2.1 Time-like Cascades

In e^+e^- annihilation, the emission of a gluon from the initial $q\bar{q}$-pair can be described in terms of dipole radiation from the colour-dipole between the q and $\bar{q}$. Subsequent emission of a second gluon is then described as radiation from either of the two dipoles connecting the quark with the gluon and the gluon with the anti-quark. In the dipole rest frame the relative probability for such a dipole splitting is to leading logarithmic order given by the standard dipole radiation formula

$$d\mathcal{P} \propto \alpha_s \frac{dk_\perp^2}{k_\perp^2} dy. \tag{2.1}$$

The available phase space is a triangular region in the $(\log k_\perp^2, y)$ plane, $k_\perp e^{\pm y} < W$, where W is the invariant mass of the dipole.

Clearly this is very similar to the Mueller dipole formalism. The main differences are that here we have dipoles in momentum space rather than in transverse position, and the evolution is in decreasing transverse momentum rather than in increasing rapidity. Hence we here have a Sudakov form factor

$$-\log \Delta_S(k_{\perp\max}^2, k_\perp^2) = \int_{k_\perp^2}^{k_{\perp\max}^2} \frac{d\mathcal{P}}{dk_\perp'^2} dk_\perp'^2. \tag{2.2}$$

Also, we here deal only with real final-state emissions, while Mueller's formalism describe initial-state virtual dipoles.

The ordering in decreasing $k_\perp$ (measured in the rest frame of the emitting dipole) means that energy and momentum conservation is a relatively small correction. This

formalism is easily implemented in a Monte Carlo generator, in which it is straight forward to take into account non-leading corrections to the emission probability in eq. (2.1) and energy-momentum conservation including proper recoils of the emitters, which modifies the triangular phase space region slightly as shown in figure 1.

This formalism has many advantages as compared to conventional parton cascades. One very essential feature is that coherence effects, conventionally implemented as angular ordering, is automatically taken into account in a way which is more accurate than the conventional sharp angular cut.

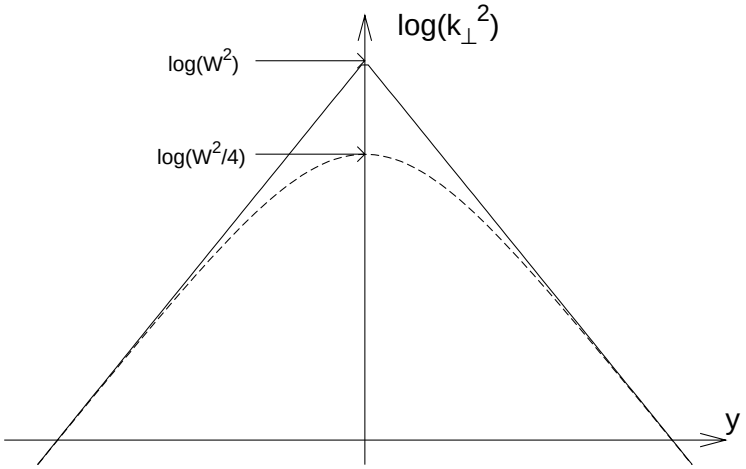

Figure 1: The available phase space for a gluon emitted with some transverse momentum $k_\perp$ and rapidity y from a dipole with total invariant mass W. The full line represents the approximate phase space limits relevant for a leading log calculation, while the dashed line represents the modification when taking recoils of the emitting quarks into account.

2.2 Space-like Cascades

The dipole cascade model has been extended to also describe deeply inelastic lepton–hadron collisions in two different ways. The one which is implemented in ARIADNE relies on a semi-classical model [42] where all gluon emissions are treated as final-state radiation. This has been very successful in describing hadronic final states at HERA, but suffers from the fact that it does not predict the cross section. It is also difficult to relate to any standard evolution equation, although it has qualitative similarities with BFKL and CCFM.

The other extension is called the Linked Dipole Chain (LDC) model [33] and uses a reformulation and generalization of CCFM evolution to build up an initial set of gluon emissions, which determines the cross section. These gluons define a chain of linked dipoles, which may initiate standard final-state dipole splittings, which then do not affect the cross section. The initial gluons are carefully selected to be purely real final-state gluons, i.e. only such emissions are considered which are not accompanied by large virtual corrections given by the so-called non-Sudakov form factor in CCFM (or Regge form factor in BFKL).

It turns out that these emissions are those where the gluons are ordered in both positive and negative light-cone momenta and with transverse momenta which are larger than the smaller of transverse momenta of the radiating propagator gluon before and after the emission: $p_{\perp i} > \min(k_{\perp i-1}, k_{\perp i})$. We are then left with simple splittings which either increase the $k_\perp$ of the propagator, given by

$$d\mathcal{P} = \bar{\alpha}\frac{dk_{\perp i}^2}{k_{\perp i}^2}\frac{dz_i}{z_i}, \tag{2.3}$$

or decreasing it, given by

$$d\mathcal{P} = \bar{\alpha}\frac{dk_{\perp i}^2}{k_{\perp i}^2}\frac{dz_i}{z_i}\frac{k_{\perp i}^2}{k_{\perp i-1}^2}. \tag{2.4}$$

The extra suppression $k_{\perp i}^2/k_{\perp i-1}^2$ for evolution with decreasing $k_\perp$ ensures that the evolution becomes symmetric, i.e. it does not matter whether we evolve from the proton or the virtual photon end. A local maximum, $k_{\perp\max}$, can be interpreted as evolutions from the projectile and target ends up to a central hard sub-collision. If treated as evolution from one end we then have a step up to $k_{\perp\max}$ followed by a step down in $k_\perp$, and from the weights in eqs. (2.3) and (2.4) this gives the correct factor $1/k_{\perp\max}^4$ expected from Rutherford scattering. If we instead have a local minimum, $k_{\perp\min}$, then there is no associated power of $k_\perp$, and such a minimum is therefore free of singularities.

Also the LDC model has been implemented in a Monte Carlo generator [41], which fairly well reproduces final states at HERA. However, there is a caveat, namely that crucial measurements sensitive to small-x dynamics, such as the rates of forward jets, can only be reproduced if non-singular parts of the gluon splitting function are omitted. For further discussions on this subject, we refer the reader to ref. [43].

3. Dipole Cascades in Coordinate Space

3.1 The Mueller Dipole Formulation

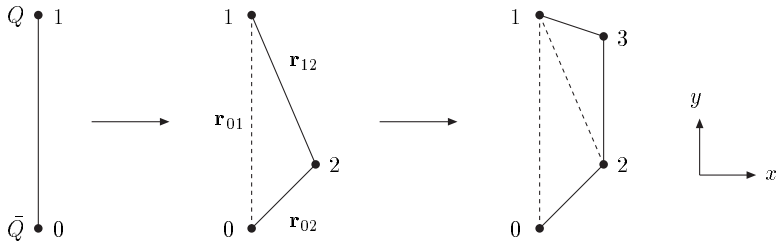

Figure 2: A quark-antiquark dipole in transverse coordinate space is split into successively more dipoles via gluon emission.

Consider now the process of an evolving onium state or $\gamma^* \to Q\bar{Q} \to Qg\bar{Q} \to Qgg\bar{Q} \to \ldots$ in transverse coordinate space, as illustrated in figure 2. Here a virtual photon is split into a $Q\bar{Q}$ colour dipole, which is first split into two dipoles by the emission of a gluon, then into three dipoles by a second gluon, etc. The probability for such a dipole splitting

is given by the expression (for notation see figure 2)

$$\frac{dP}{dy} = \frac{\bar{\alpha}}{2\pi} d^2\mathbf{r}_2 \frac{r_{01}^2}{r_{02}^2\, r_{12}^2} \cdot S$$
$$\text{where } S = \exp\left[-\frac{\bar{\alpha}}{2\pi}\int dy \int d^2\mathbf{r}_2 \frac{r_{01}^2}{r_{02}^2\, r_{12}^2}\right]. \tag{3.1}$$

Here S denotes a Sudakov form factor. When this dipole splitting is iterated it evolves into a cascade with with an exponentially increasing number of dipoles.

We note that the weight in eq. (3.1) is singular, and the integral over $d^2\mathbf{r}_2$ in the Sudakov form factor diverges for small values of r_{02} and r_{12}. Therefore Mueller introduced a cutoff ρ, such that the splitting has to satisfy $r_{02} > \rho$ and $r_{12} > \rho$. The integral in S is then also restricted in the same way. A small cutoff value ρ will here imply that we get very many dipoles with small r-values. However, as the cross section for a small dipole interacting with a target also gets small (see below), the total cross section is finite also in the limit $\rho \to 0$.

A proton target can be treated as a collection of dipoles. When two dipoles collide, there is a recoupling of the colour charges, forming new dipole chains. This is schematically illustrated in figure 3 for the case of $\gamma^\star\gamma^\star$ scattering. Here we imagine the two virtual photons splitting up into quark-antiquark pairs, which develop into two colliding dipole cascades. When the two central dipoles collide, it implies a recoupling, as indicated by the arrow. The weight for this interaction is given by the expression [32]

$$f = \frac{\alpha_s^2}{2}\left\{\log\left[\frac{|\mathbf{r}_1 - \mathbf{r}_3| \cdot |\mathbf{r}_2 - \mathbf{r}_4|}{|\mathbf{r}_1 - \mathbf{r}_4| \cdot |\mathbf{r}_2 - \mathbf{r}_3|}\right]\right\}^2. \tag{3.2}$$

An important property of this expression is that when e.g. the left of the interacting dipoles is small, the weight in eq. (3.2) can be shown to be proportional to $(\mathbf{r}_1 - \mathbf{r}_2)^2$, which compensates the factor $(\mathbf{r}_1 - \mathbf{r}_2)^{-2}$ in the evolution probability from eq. (3.1).

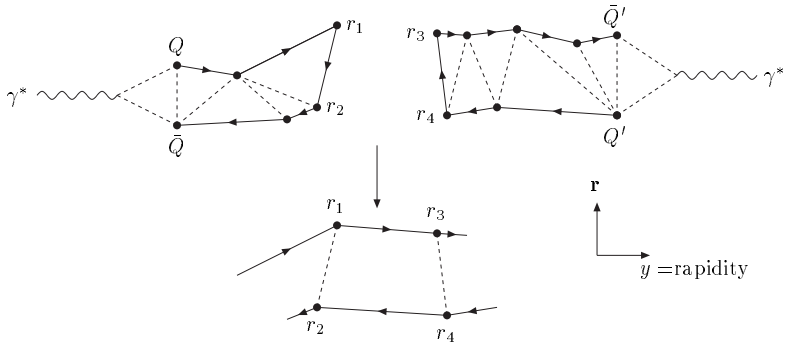

Figure 3: A symbolic picture of a $\gamma^*\gamma^*$ collision in rapidity-$\mathbf{r}_\perp$-space. The two dipole chains interact and recouple with probability f given by eq. (3.2).

A $\gamma^\star p$ collision is frequently analyzed in the rest frame of the target proton. When the virtual photon hits the target, the number of dipoles present in this frame grows in

accordance with the BFKL equation, and the total cross section increases proportional to $\exp(\lambda Y)$, where the total rapidity interval Y is given by $Y = \log(1/x) = \log(s/Q^2)$.

It is, however, also possible to study the collision in a frame different from the target rest frame. Then the target dipoles evolve in the same way a distance y in rapidity, while the projectile dipole evolves the shorter distance $Y - y$. As the evolution grows exponentially with rapidity, the cross section is proportional to $\exp(\lambda y) \cdot \exp(\lambda(Y-y)) = \exp(\lambda Y)$, which means that it is insensitive to the chosen frame, in which the collision is studied. This frame independence is, however, broken by multiple collision effects related to unitarity. This will be discussed further in section 4.4.

3.2 Unitarity and Saturation

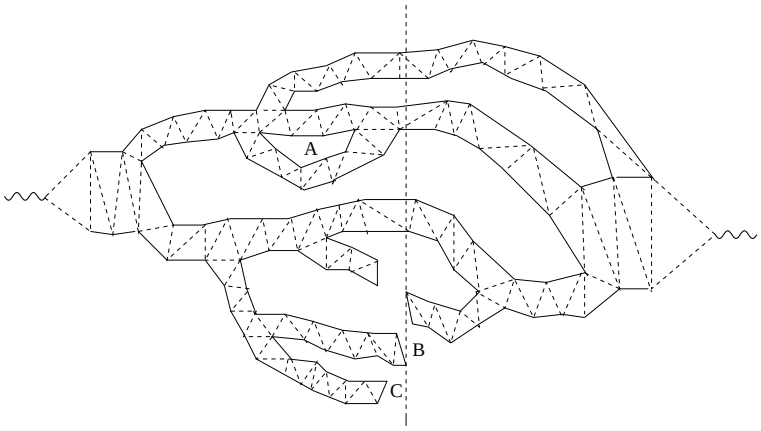

Figure 4: A $\gamma^\star\gamma^\star$ collision event with multiple sub-collisions in rapidity-$\mathbf{r}_\perp$-space. At high energies several branches from the two colliding dipole systems may reconnect. The dashed vertical line symbolizes the Lorentz frame in which the collision is evaluated.

A great advantage of the coordinate space representation is the fact that the transverse coordinate $\mathbf{r}$ is unchanged during the collision. This implies that unitarity can very easily be implemented by the replacement $f \to 1 - e^{-f}$. As the dipole cascades from the two virtual photons branch out, it is also possible to have *multiple interactions* with dipoles from the left and from the right, as illustrated in figure 4. The total cross section is then given by

$$\sigma \propto \int d^2\mathbf{b}(1 - e^{-\sum f_{ij}}). \tag{3.3}$$

where $\mathbf{b}$ denotes the impact parameter separation between the two initial particles, and the sum runs over all pairs i and j of colliding dipoles. Here the factor $1 - e^{-\sum f_{ij}}$, where the exponent corresponds to a no-interaction probability, ensures that the unitarity constraint is satisfied. The first term in an expansion, $\sum f_{ij}$, corresponds to a single pomeron exchange, while the higher order terms are related to multi-pomeron exchanges.

Including these non-linear terms in the evolution equation leads to the Balitsky–Kovchegov (BK) equation [10, 11]. The BK equation governs the small-x evolution of the F_2 structure function of a large nucleus. In his original paper Kovchegov assumed a

target nucleus at rest and an evolved projectile dipole. Using Mueller's dipole formulation for the evolution of the dipole and summing pomeron exchanges of all orders he derived the following equation:

$$\frac{dN(\mathbf{r}_{01},Y)}{dY} = \frac{\bar{\alpha}}{2\pi}\int d^2\mathbf{r}_2 \frac{r_{01}^2}{r_{02}^2 r_{12}^2}(N(\mathbf{r}_{12},Y)+N(\mathbf{r}_{02},Y)-N(\mathbf{r}_{01},Y)-N(\mathbf{r}_{12},Y)N(\mathbf{r}_{02},Y)). \tag{3.4}$$

Here $N(\mathbf{r}_{ij},Y)$ denotes the forward scattering amplitude (which also determines the total reaction probability) of the dipole $\mathbf{r}_{ij}$ on the target nucleus. The nucleus has been assumed to be large, which means that the impact parameter dependence of N is suppressed.

For small N-values the quadratic term can be neglected, and eq. (3.4) is reduced to Mueller's linear equation for the dipole cascade evolution. This equation is just the BFKL equation formulated in the dipole language. The first two terms correspond to the emission of a gluon forming two new dipoles, while the term with a minus sign accounts for the virtual corrections described by the Sudakov form factor in eq. (3.1). The quadratic term represents the effect of multiple collisions, which become more important when N becomes large. This suppresses the growth rate for larger Y-values and results in saturation when N approaches 1, thus preserving unitarity.

The BK equation (3.4) describes the development of the cascade before it hits a dense nuclear target. It can also be used to describe the evolution of two colliding cascades in a $\gamma^\star\gamma^\star$ collision, as illustrated in figure 4. Here several branches from the two systems may reconnect as described in figure 3 and eq. (3.2). We note here that the cascade evolution described by the linear terms in eq. (3.4) are only leading in colour, while the effect from multiple collisions is formally colour suppressed. Therefore this formalism includes corrections from multiple sub-collisions in the Lorentz frame in which the process is evaluated (denoted by the vertical dashed line in figure 4), but does not take into account the possibility that two branches recombine before the collision. Such an event is indicated by the letter A in figure 4. This effect is also colour suppressed and thus not included in the evolution. As a consequence the result depends on the Lorentz frame used, and this problem will be further discussed in section 4.4.

4. Combining Energy-Momentum Conservation and Unitarity

With a small cutoff ρ ($r > \rho$) we get, as mentioned above, very many small dipoles. If these are interpreted as real emissions, with transverse momenta proportional to $1/r$, it would imply a catastrophic violation of energy-momentum conservation. As discussed above, the emission of these small dipoles have a very limited effect on the total cross section, and they have to be interpreted as virtual fluctuations. Thus the result in eq. (3.3) will describe the inclusive cross section, but the many dipoles produced in all the branching chains will not correspond to the production of exclusive final states.

4.1 Relation Mueller's Dipole Cascade vs. LDC

Before a discussion of these virtual fluctuations we want to discuss the relation between Mueller's Dipole Cascade and the LDC model. Let us study the chain of emissions, which

is illustrated in figure 5. Apart from the Sudakov factors this chain gets the following weight:

$$\frac{d^2\mathbf{r}_2\, r_{01}^2}{r_{02}^2\, r_{12}^2}\cdot\frac{d^2\mathbf{r}_3\, r_{12}^2}{r_{13}^2\, r_{23}^2}\cdot\frac{d^2\mathbf{r}_4\, r_{23}^2}{r_{24}^2\, r_{34}^2}\cdot\frac{d^2\mathbf{r}_5\, r_{34}^2}{r_{35}^2\, r_{45}^2}\cdot\frac{d^2\mathbf{r}_6\, r_{35}^2}{r_{36}^2\, r_{56}^2} = \\ = r_{01}^2\frac{d^2\mathbf{r}_2\, d^2\mathbf{r}_3\, d^2\mathbf{r}_4\, d^2\mathbf{r}_5\, d^2\mathbf{r}_6}{r_{02}^2\, r_{13}^2\, r_{24}^2\, r_{45}^2\, r_{36}^2\, r_{56}^2} \tag{4.1}$$

We here note that the total weight is a product of factors $1/r_{ij}^2$ for all *"remaining dipoles"*, i.e. for those dipoles which have not been split by further gluon emission. They are marked by solid lines in figure 5. All dependence on the size of *"intermediate"* dipoles, which have disappeared because they split in two daughter dipoles, is canceled in eq. (4.1), as they appear both in the numerator and in the denominator. (These dipoles are marked by dashed lines in figure 5.)

If a dipole size, $\mathbf{r}$, is small, it means that the gluons are well localized, which must imply that transverse momenta are correspondingly large. This implies that not only the new gluon gets a large $k_\perp \sim 1/r$, but also that the original gluon, which is close in coordinate space, gets a corresponding recoil. For the special example in figure 5 the emissions of the gluons marked 2, 3, and 4 give dipole sizes which become smaller and smaller, $a >> b >> c >> d$, in each step of the evolution. (This also implies that the "remaining" and the "intermediate" dipoles are pairwise equally large.) The corresponding $k_\perp$-values therefore become larger and larger in each step. After the minimum dipole, with size d, the subsequent emissions, 5, and 6, give again larger dipoles with correspondingly lower $k_\perp$ values. The probability for this chain is proportional to

$$\frac{d^2\mathbf{r}_2}{b^2}\cdot\frac{d^2\mathbf{r}_3}{c^2}\cdot\frac{d^2\mathbf{r}_4}{d^0}\cdot\frac{d^2\mathbf{r}_5}{e^2}\cdot\frac{d^2\mathbf{r}_6}{f^2}\cdot\frac{1}{f^2} \tag{4.2}$$

For the first emissions, 2 and 3, we in this expression recognize the product of factors $\prod d^2\mathbf{r}_i/r_i^2 \propto \prod d^2\mathbf{k}_i/k_i^2$, just as is expected from a "DGLAP evolution" of a chain with monotonically increasing $k_\perp$. Emission number 4 corresponds to the minimum dipole size, d, which should be associated with a maximum $k_\perp$. In the following evolution the dipole sizes get larger again, corresponding to successively smaller transverse momenta. In analogy with the evolution in the LDC model described in section 2.2, this latter part can be interpreted as DGLAP evolution in the opposite direction, i.e. from the target end up to the central hard sub-collision. In this sub-collision the gluons 3 and 4 recoil against each other with transverse momenta $k_{\perp\max}$. In eq. (4.2) we see that the factors of d have canceled, which thus gives the weight $d^2\mathbf{r}_4 \propto d^2\mathbf{k}_{\max}/k_{\max}^4$. This reproduces the weight expected from a hard gluon–gluon scattering, and corresponds exactly to the result in the LDC model as discussed in section 2.2.

Figure 6 shows instead a chain with increasing dipole sizes up to a maximum value, $r_{\max}$, which thus corresponds to a minimum transverse momentum, $k_{\perp\min}$. Here we get the weight $d^2\mathbf{r}_{\max}/r_{\max}^4 \propto d^2\mathbf{k}_{\min}$. Therefore there is no singularity for the minimum $k_\perp$-value. This result is also directly analogous to the corresponding result in the LDC model.

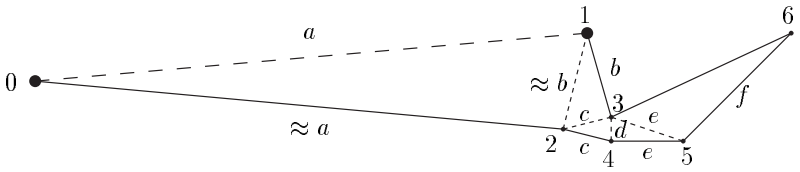

Figure 5: A dipole cascade in rapidity-$\mathbf{r}_\perp$-space, where a chain of smaller and smaller dipoles is followed by a set of dipoles with increasing sizes. The initial dipole between points 0 and 1 is marked by long dashes, and those dipoles which have split into two new dipoles and disappeared from the chain are marked by short dashes. This chain is interpreted as one $k_\perp$-ordered cascade from one side and one from the other, evolving up to a central hard sub-collision, which is represented by the dipole with minimum size and therefore maximum $k_\perp$.

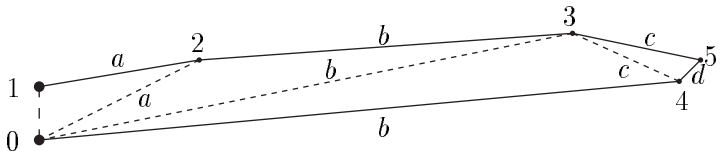

Figure 6: A cascade where the dipoles increase to a maximum, and then decrease. Here the size of the largest dipole, denoted b, corresponds to the minimum $k_\perp$ in the chain.

4.2 Energy-Momentum Conservation

As discussed in section 2.2, the main feature of the LDC model is the observation that both the total cross section and the final state structures are determined by chains consisting of a subset of the gluons appearing in the final state. These gluons were called "primary gluons" in ref. [33] and later called "backbone gluons" in ref. [44]. Remaining real final state gluons can be treated as final state radiation from the primary gluons. Such final state emissions do not modify the total cross sections, and give only small recoils to the parent emitters. The primary gluons have to satisfy energy-momentum conservation, and are ordered in both positive and negative light-cone momentum components, p_+ and p_-. We saw in the previous section that in Mueller's cascade the emission probabilities for gluons, which satisfy the conditions for primary gluons in LDC, have exactly the same weight, when the transverse momenta are identified with the inverse dipole size, $2/r$. This inspires the conjecture that with this identification an appropriate subset of the emissions in Mueller's cascade can correspond to the primary gluons in the momentum space cascade, meaning that they determine the cross sections while the other emissions can be regarded as either virtual fluctuations or final state radiation.

A necessary condition for this subset of gluons is that energy and momentum is conserved. (This is not a sufficient condition, as discussed further below.) Only emissions which satisfy energy-momentum conservation can correspond to real emissions, and keeping only these emissions (with a corresponding modification of the Sudakov form factor) gives a closer correspondence between the generated dipole chains and the observable final

states. To leading order this does not change the total cross section. However, as it has been demonstrated that a large fraction of the next to leading corrections to the BFKL equation is related to energy conservation, we expect that taking this into account will improve the results also in this dipole formulation of the evolution.

A very important consequence of energy-momentum conservation is also that it implies a *dynamical cutoff*, $\rho(\Delta y)$, which is large for small steps in rapidity[2], Δy, but gets smaller for larger Δy. (Alternatively it could be described as a cutoff for Δy which depends on r.) The production of a small dipole with size r corresponds to the emission of a gluon with $k_\perp \approx 2/r$ and therefore $k_+ \approx (2/r)e^{-y}$. Thus conservation of positive light-cone momentum implies

$$r > 2e^{-\Delta y}/k_{\perp\text{parent}}. \tag{4.3}$$

Conserving also the negative light-cone momentum, p_-, implies that we in a similar way also get a maximum value for r in each emission. Here we note that while the projectile has a large p_+ component and a very small p_- component, the target has small p_+ but contributes (almost) all p_-. Thus conservation of p_- means that in the evolution of the projectile cascade, the p_- components become steadily larger, presuming that in end the collision with the target will provide the total p_- needed to put the cascade on shell. (The kinematical details will be discussed further in section 5.) Branches which do not interact must consequently be regarded as virtual fluctuations, which are not realized in the final state.

The net result of conservation of both p_+ and p_- is that the number of dipoles grows much more slowly with energy, and we will see in section 6 that this also strongly reduces the total cross sections. Besides this physical effect, it also simplifies the implementation in a MC program, and implies that the severe numerical complications encountered in MC simulations without energy conservation, discussed in refs. [32] and [31], can be avoided.

4.3 Final States and Virtual Dipoles

However, even if we only include emissions which would be allowed by energy-momentum conservation, this does not fully correspond to the formation of a possible final state. As discussed above, the weight contains in the denominator the square of all "remaining dipoles". Even if the constraint from energy-momentum conservation implies a minimum rapidity gap for the emission of small dipoles, this suppression does not reproduce the weight $\propto d^2k_\perp/k_\perp^4$ for the smallest dipole in a sequence, needed to reproduce the cross section for a hard sub-collision. A possible solution is to interprete clusters of gluons, like those marked A, B, and C in figure 7, as "effective gluons", where the small internal separations do not correspond to large transverse momenta for real final state gluons. These hard emissions have to be compensated by virtual corrections.

From the weight in eq. (3.1) we see that that the emission probability, where such a small dipole is the parent, is proportional to the square of its length, and therefore suppressed. However, if this dipole really does split by gluon emission, and starts a branch which interacts and gets coupled to a chain from the target (as illustrated in figure 8) then

[2]Note that in our notation, y is rapidity and not $\log(1/x)$.

the separation cannot be neglected. In this case the two gluons at the dipole ends have to be treated as independent, and can no longer be considered as a single effective gluon. This problem concerning the properties of exclusive final states will be further discussed in a forthcoming publication, and in the following we will here only discuss results for total cross sections.

A very important question concerns whether demanding energy conservation also for virtual emissions implies a serious overestimate of its consequences. The production of a small dipole implies large $p_\perp$ for the new gluon and also for its partner in the dipole, which suffers a recoil. Since the new dipole can be virtual only if it does not interact further, this is a problem if the neighbouring dipoles are significantly changed by the emission. In the calculations of the effect of the recoil, the lightcone component $p_+ = e^{-y} \cdot p_\perp$ is conserved, which implies that the rapidity y is adjusted to a larger value. This implies that the emission of the virtual dipole does not significantly modify the p_+-component of the neighbouring dipoles. It does, however, have a large effect on the values of $p_- = e^{+y} \cdot p_\perp$, where the changes in $p_\perp$ and y do not compensate each other. In order not to overestimate the effect of p_--conservation, we therefore in this analysis implement the constraint from p_--conservation in such a way, that we neglect the size of the neighbouring dipoles. Thus we calculate this constraint assuming that the $p_\perp$ of the gluons in the dipole ends is determined only by the size of the emitting dipole. This does somewhat underestimate the effect of p_--conservation, but it avoids the large overestimate, which would be the consequence of including the unrealistic constraint from virtual dipole neighbours.

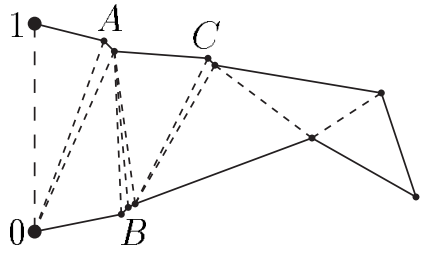

Figure 7: The clusters of gluons marked A, B, and C must be interpreted as "effective gluons". The small dipole sizes do not correspond to large final state transverse momenta.

4.4 Gluon Recombination and Frame Dependence

As mentioned in section 3.1 the resulting cross section is relatively insensitive to the reference frame in which a collision is studied. If the interaction is studied in a frame with rapidity y relative to the projectile, then (in leading order) the projectile cascade has evolved by a factor $e^{\lambda y}$ and the cascade from the target by a factor $e^{\lambda(Y-y)}$, where Y represents the total rapidity interval. The product is proportional to e^Y, and thus independent of y. It is also demonstrated in ref. [31] that the result for a single chain is the same in all frames, and independent of whether the cascades are developed from the projectile end or

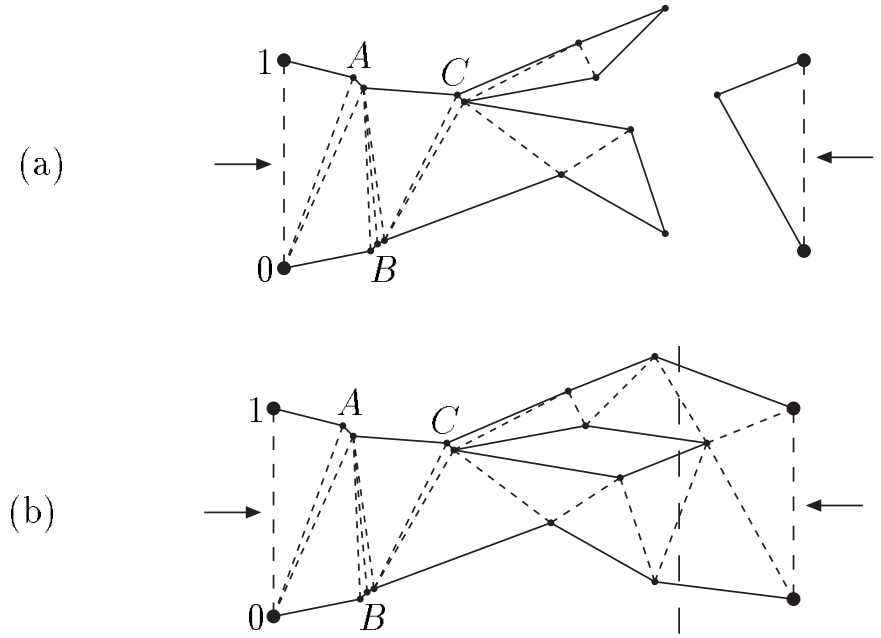

Figure 8: (a) The emission of a new branch from a small dipole is suppressed, and proportional to the square of the small dipole size. However, if such a branch is emitted and interacts with a dipole from the target (b), then the small size has to correspond to a large $k_\perp$ in the final state.

from the target end. This is a consequence of the Möbius invariance of the process, and is exactly true in the limit when the cutoff ρ goes to zero.

However, including the unitarity corrections from multiple collisions also implies that the result is no longer frame independent. The contributions from multiple collisions in eq. (3.3) are formally colour suppressed $\sim 1/N_c^2$. What is treated as a multiple collision in figure 4 or 8 corresponds in the target rest frame to a process where two dipoles fuse to a single dipole (or two gluons fuse to a single gluon) before the collision with the target. Such recombinations[3] are consequently also colour suppressed, and they are not included in the dipole cascade evolution, which is only leading order in N_c. In the final state this process gives a closed dipole loop, which is colour disconnected from the rest of the system. In a string fragmentation scenario it gives a closed string, which fragments as a separate system. This implies that such loops are only taken into account if the collision is studied in a frame where they are appearing as multiple collisions between two branches coming from each direction, and not in a frame where they appear as gluon recombination, as e.g. in the target rest frame.

We conclude that within this formalism the unitarisation corrections *do* depend on the Lorentz frame used. As discussed in ref. [31], for symmetric collisions the optimal frame

[3] In the terminology of ref. [31] the effect of multiple collisions is called a unitarisation effect, while the effect of gluon recombination is called saturation. As the separation between the two mechanisms is not dynamical, but only a question of bookkeeping depending on the particular frame of reference used in the analysis, we do in this paper not make this distinction.

should be the overall rest system, where both the projectile and the target may evolve, and the probability is largest that a dipole loop corresponds to a multiple collision event. This is illustrated in figure 4, where in the overall rest system only one loop does not correspond to a multiple collision but to a gluon recombination. In a less central frame more loops would correspond to recombinations and there would be correspondingly fewer multiple sub-collisions.

The situation is different for onium scattering on a dense nuclear target. Here the target is treated as a large number of dipoles, and multiple collisions are most likely when different initial dipoles from the target are involved. Therefore multiple collisions are well accounted for in the target rest frame, where the projectile cascade is fully developed. This is also the approach taken in the BK equation, which similarly takes into account multi-pomeron exchange but not the gluon recombination process representing pomeron fusion.

The frame independence is a very essential feature of the LDC model, and we think it is important to develop a formalism in which multiple collisions and gluon recombinations appear on an equal footing, in a frame independent description. We will return to this problem in a future publication.

There is also another frame dependent effect, which has a more kinematic origin. For a finite cutoff ρ, or for the effective cutoff $\rho(\Delta y)$, the frame independence is only approximate, also for a single chain. Furthermore, in our scheme for energy conservation every new branch takes away energy, and therefore in a cascade with many branches the energy in each individual branch is reduced. As discussed in section 4.2, a branch can only be realized if the interaction with the target can provide the necessary p_- momentum. The other branches are virtual and cannot be realized in the final state. This is e.g. the case for the branches marked B and C in figure 4. As our constraint from energy-momentum conservation also includes the fractions needed to evolve the non-interacting branches the effect is somewhat overestimated. Quantitatively this bias turns out to be small. For dipole–dipole collisions, as described in section 6.2, we find that the cross sections calculated in the cms at $y = 0.5\,Y$ or asymetrically at $y = 0.75\,Y$ differ by less than 4%.

5. The Monte Carlo Implementation

In this section we briefly describe the Monte Carlo scheme used to calculate the results presented in this paper. As we have mentioned before, the onium state is evolved in rapidity. For a given dipole one then generates y and $\mathbf{r}$ values for a possible gluon emission (dipole splitting) using eq. (3.1).

5.1 Kinematics

To be able to study the effects of energy-momentum conservation we simply assign besides a transverse position and a rapidity, a positive light-cone momentum and a transverse momentum to each parton in the evolution, where $k_+ = k_\perp e^{-y} = (2/r)e^{-y}$. The dynamical cutoff is then given by $\rho = 2e^{-\Delta y}/k_{\perp\mathrm{parent}}$. When a dipole emits a gluon the mother partons

will receive recoils from the emitted gluon. Since a gluon belongs to two different dipoles one has to decide how the emission of a gluon effects the neighboring dipoles. We will simply assume that when a dipole emits a gluon the mother gluons need to supply all the needed energy. Thus the next time a neighboring dipole emits a gluon, the avaliable energy is reduced because one of its gluons has lost energy from the earlier emission.

Consider the emission of gluon n from the dipole ij between partons with light-cone momenta k_{+i} and k_{+j}. The transverse distances between the new gluon and partons i and j are denoted r_{in} and r_{jn} respectively. We then assume that the nearest parent gluon takes the dominant fraction of the recoil. Thus if k_{+n} is the momentum given to the emitted gluon, then the momenta left to the parents after the emission are given by

$$k'_{+i} = k_{+i} - \frac{r_{jn}}{r_{jn}+r_{in}} k_{+n} \quad \text{and} \quad k'_{+j} = k_{+j} - \frac{r_{in}}{r_{jn}+r_{in}} k_{+n}. \tag{5.1}$$

Alternative formulas for sharing the recoils have also been studied, but the result does not depend sensitively on the exact formula. When an emission is generated we always make sure that $k'_+ \geq 0$.

As we in this paper are not investigating final state properties but only total cross sections, we will neglect the directions of the transverse momenta. Keeping only the lengths of the $\mathbf{k}_\perp$ vectors, we neglect the possibility that two contributions may be of approximately equal size in opposite directions, giving a much smaller vector sum. This approximation has to be improved in future analyses of final states, but should not be essential here. Thus in our approximation the transverse momentum of a parton will be decided by the shortest distance to another parton, with which it has formed a dipole, and when the gluon n is emitted from the dipole (ij), its transverse momentum is given by

$$k_{\perp n} = 2\max\left(\frac{1}{r_{in}}, \frac{1}{r_{jn}}\right). \tag{5.2}$$

In analogy the recoils on the emitting partons are given by

$$\begin{aligned} k'_{\perp i} &= \max\left(k_{\perp i}, \frac{2}{r_{in}}\right) \\ k'_{\perp j} &= \max\left(k_{\perp j}, \frac{2}{r_{jn}}\right). \end{aligned} \tag{5.3}$$

The recoil also implies that the rapidity is modified for the parents, and is determined by the relation $y' = \log \frac{k'_+}{k'_\perp}$. In some cases this could imply that an emitting parton ends up with rapidity larger than the rapidity of the emitted gluon. Since the cascade is assumed to be ordered in rapidity, such emissions are not allowed, and we demand that $y'_i, y'_j \leqslant y_n$. In this way we also avoid the situation where there are partons which have rapidities outside the allowed rapidity interval. As mentioned in section 4.2, negative light-cone momentum is also conserved. This we do by imposing the condition $k_{-n} \geqslant \max(k_{-i}, k_{-j})$ during the evolution, where $k_{-i} = 2e^{y_i}/r_{ij}$ and $k_{-j} = 2e^{y_j}/r_{ij}$ according to the discussion in section 4.3. For every generated gluon one checks the kinematical constraints described above, and in case one of them is not satisfied a new gluon is generated in a way which automatically includes the same phase-space restrictions in the integral of the Sudakov form factor.

The constraint on the negative light-cone momentum given above implies that k_- steadily increases. As also discussed in section 4.2 we presume that in the end the collision with the target provides the necessary k_- to put the dipole chain on shell. To make sure that this indeed is possible, we impose the following constraint on the colliding dipoles

$$\frac{16}{r_{ab}^2} < k_{+a} \cdot k_{-b} \tag{5.4}$$

Here a and b denote two colliding gluons, which are connected in the recoupling as shown in figure 3. The left moving onium is the one with larger k_- while the right moving onium has larger k_+. When two dipoles collide there is only one possible way to reconnect the gluons, which is consistent with the colour flow. The constraint in eq. (5.4) has to be satisfied for both pairs of connected gluons. If one of the constraints is not satisfied, the corresponding scattering amplitude is set to zero, which guarantees that only sub-collisions, which satisfy energy-momentum conservation, contribute to the cross section.

As a final remark we mention that all calculations are performed using a fixed coupling constant α_s, corresponding to $\bar{\alpha} = 0.2$. We intend to study the effects of a running coupling in future investigations.

6. Results

6.1 Dipole Multiplicity

We will begin this section by describing some of the general properties of the dipole evolution, and we first study how the dipole multiplicity grows with energy. In figures 9 and 10 we show the average number of dipoles with and without energy conservation. As some dipoles have to be regarded as virtual, according to the discussion in section 4.3, these results do not have a direct physical interpretation. They are interesting because they may be helpful, e.g. in estimates of effects of multiple collisions and the efficiency of the MC program. Without energy conservation a fixed cutoff, ρ, is needed for small dipole sizes, and in figure 10 results are shown for $\rho = 0.04\, r_0$ and $\rho = 0.02\, r_0$, where r_0 is the size of the initial dipole starting the cascade. In all cases the total dipole multiplicity is growing exponentially with rapidity. A small cutoff favors the production of very many small dipoles, which is reflected in a very large dipole multiplicity, as seen in figure 10. With energy conservation the dynamical cutoff $\rho(\Delta y)$, discussed in section 4.2, is large for small values of Δy, and this feature effectively suppresses the production of many small dipoles in a small rapidity interval. Comparing the two figures we see that energy conservation indeed does have a very large effect. With energy conservation the multiplicity at $Y \approx 10$ is a factor 20 below the result obtained including energy conservation with the smaller cutoff value.

Without energy conservation the strong sensitivity to the small dipole cutoff reflects the large probability to emit very small dipoles (c.f. eq. (3.1)). As the small dipoles also have small cross section, one could imagine that the differences seen in the dipole multiplicity is rather unessential for total cross sections. This is, however, not the case. In figures 9 and 10 we also show the number of dipoles with sizes larger or equal to the initial dipole size. With

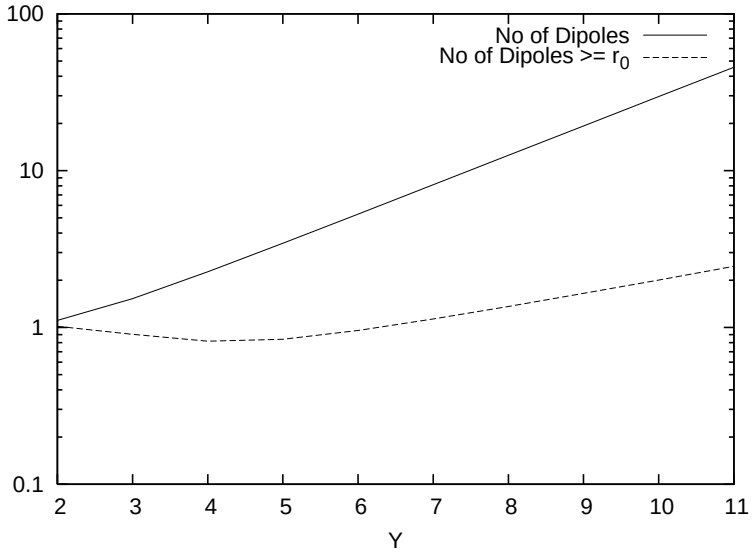

Figure 9: The average total number of dipoles (full line) together with the average number of large dipoles (dashed line) in the onium state when evolved with energy conservation.

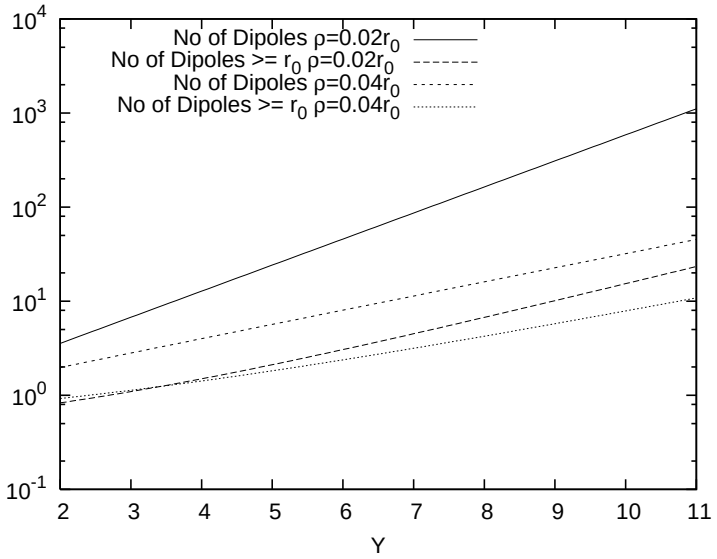

Figure 10: The average total number of dipoles together with the average number of large dipoles in the onium state when evolved *without* energy conservation and using two different cutoffs. For the smaller cutoff, $\rho = 0.02$ the total number is given by the full line while the number of large dipoles is given by the dashed line. For the larger cutoff, $\rho = 0.04$ the total number is given by the short-dashed line while the number of large dipoles is given by the dotted line.

energy conservation this number changes rather slowly and exceeds one first at $Y \sim 7$, while without energy conservation it is steadily increasing with energy. This is the case also for the larger cutoff value, although in this case the total multiplicity is not significantly larger than in the energy conserving case. This feature is further illustrated in figure 11, which shows the distribution in dipole size at $Y = 6$ and $Y = 8$. Energy-momentum conservation

does not only suppress small dipoles, which we understand as a result of conservation of the positive light-cone component, p_+, but there is also a suppression of large dipoles, as a consequence of p_--conservation. Thus we conclude that the implementation of energy conservation does not only have an effect on very small dipoles, which turns out to be less unimportant for the total cross sections, but indeed also has a very strong effect on the main features of the evolution. This will be more clearly illustrated in the following subsections.

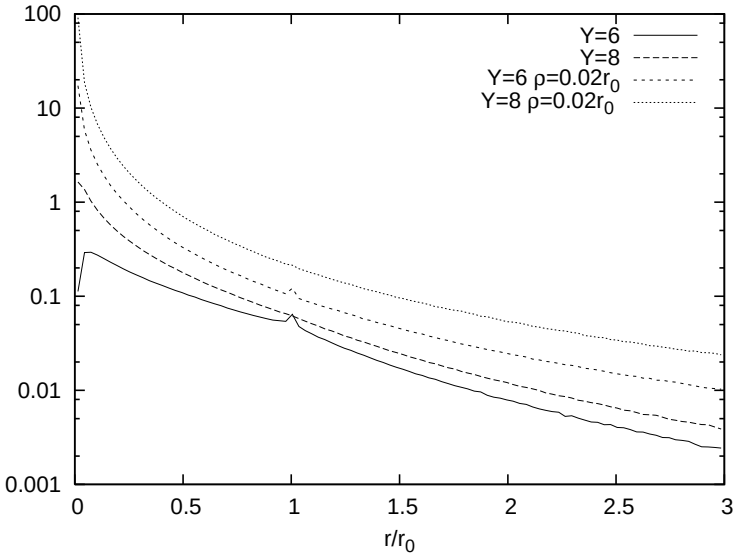

Figure 11: The distribution in dipole size for $Y = 6$ and 8. The solid and longdashed lines show the result from evolution with energy conservation while the shortdashed and dotted lines show the same for evolution *without* energy conservation with the cutoff $\rho = 0.02\, r_0$.

6.2 Onium–Onium scattering.

We will here study the collision between two onium states, which we regard as two incoming dipoles. We denote the initial dipole sizes r_1 and r_2 respectively, and we imagine r_2 as the target dipole with fixed size, while we vary the projectile size $r_1 \propto 1/\sqrt{Q^2}$. We note that with energy conservation and fixed α_s there is no external scale, and therefore the result for the scaled cross section σ/r_2^2 does not depend on r_1 and r_2 separately, but only on their ratio.

Figure 12 shows the total cross section as a function of the rapidity Y for different values of r_1/r_2, obtained including energy conservation and unitarisation in accordance with eq. (3.3). The result from single pomeron exchange, where the parenthesis in eq. (3.3) is replaced by $\sum f_{ij}$, is shown in figure 13, and we see that these results are almost identical to those in figure 12. We note in particular that the curves are not straight lines, as is expected from leading order BFKL. This implies that the effective slope, λ_{eff}, varies with rapidity, in a way expected as a result of saturation. We also note that λ_{eff} grows with larger values for the ratio between the dipole sizes. This effect is illustrated in figure 14, and will be further discussed in section 6.4.

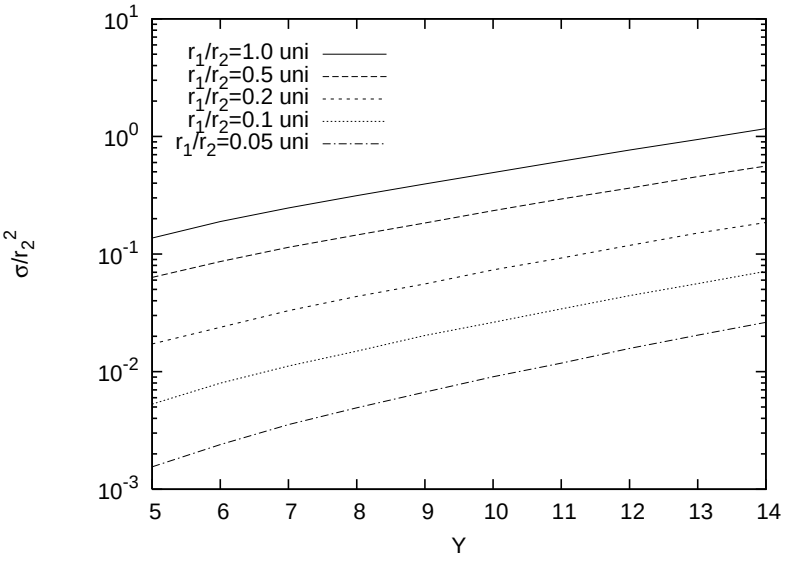

Figure 12: The scaled unitarised dipole–dipole cross section as a function of Y for different initial conditions.

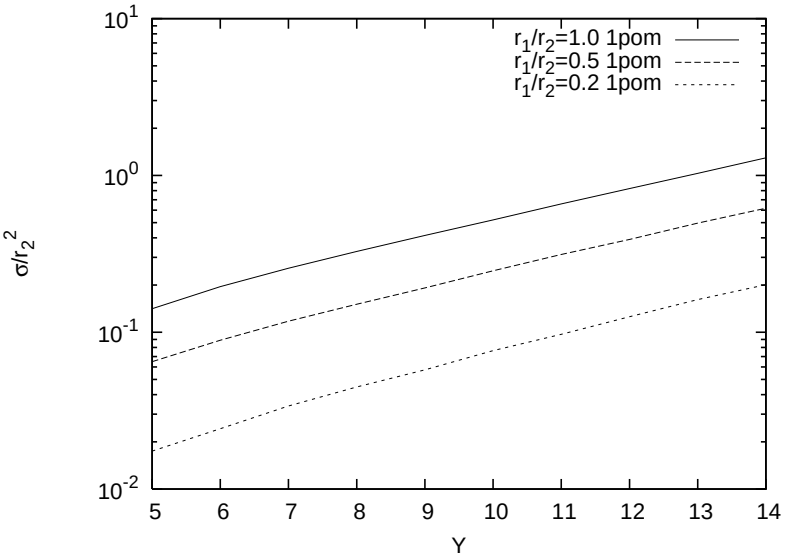

Figure 13: The scaled one-pomeron dipole–dipole cross section as a function of Y for different initial conditions.

For comparison, results obtained without energy conservation, with and without unitarisation, are shown in figure 15. In this figure the ratio r_1/r_2 is chosen equal to 1. We see that here the one-pomeron cross section, without unitarisation, grows exponentially with rapidity, proportional to $e^{\lambda Y}$ with a constant slope λ. Including unitarisation gives here a noticeable suppression, which becomes stronger for larger rapidity and correspondingly higher dipole density. This has the expected effect that the growth rate is reduced for larger rapidities, with an effective slope parameter λ_{eff} which is decreasing for higher energies. Comparing figures 12 and 13 we note that already without unitarisation, the inclusion of

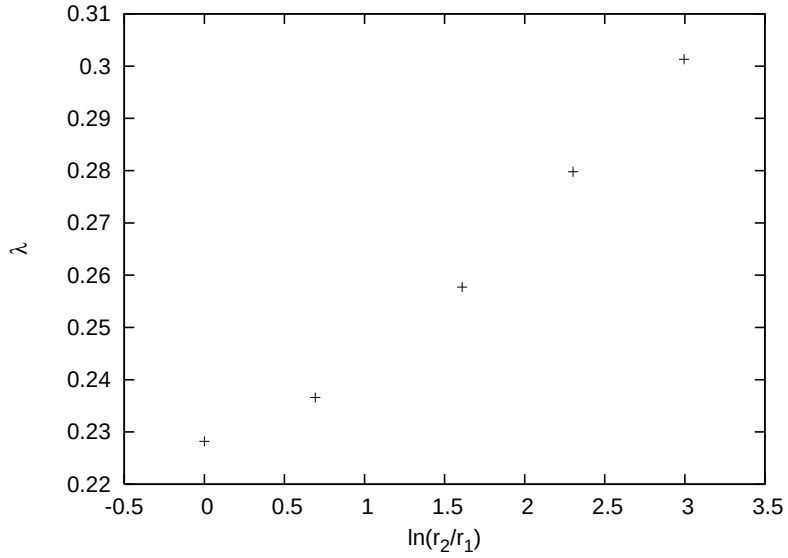

Figure 14: The effective power $\lambda_{\rm eff}$ calculated from the unitarised dipole–dipole cross section where energy conservation has been included.

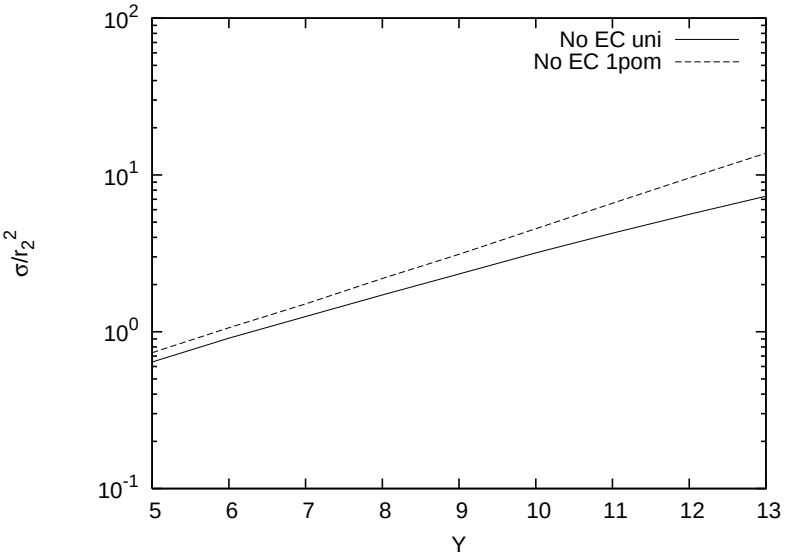

Figure 15: The scaled unitarised (full line) and one-pomeron (dashed line) dipole–dipole cross sections calculated *without* energy conservation.

energy conservation also results in an effective slope, which is varying with energy in much the same way.

6.3 Dipole–nucleus scattering.

Having studied dipole–dipole collisions we now apply our program to dipole–nucleus collisions. We will focus on the qualitative features and consider a toy model where the nucleus is given by a collection of colour dipoles, which are distributed with a Gaussian distribution in dipole size **r** and in impact parameter **b** and with random relative angles. The number

density of dipoles is given by

$$dN = B \cdot d^2\mathbf{r} e^{-\mathbf{r}^2/r_0^2} \cdot d^2\mathbf{b} e^{-\mathbf{b}^2/b_0^2} \tag{6.1}$$

The parameters r_0 and b_0 are related to the estimated primordial momentum in a proton and the nuclear radius respectively. As our model is rather crude we have not tried to optimize these parameters, but chosen the following canonical values: $r_0 = 1$ fm and $b_0 = A^{1/3} \cdot 1$ fm, A being the mass number for the nucleus. The normalization constant B is determined by the requirement that the transverse energy of the nucleus is set equal to $A \cdot 1$ GeV. To simplify the calculations, the interaction amplitude for a dipole–nucleus collision is calculated in the nucleus rest frame, by convoluting the basic dipole–dipole amplitude with the distribution in eq. (6.1). Although, as discussed in section 4.4, the result is not exactly independent of the Lorentz frame, the differences are not large, and should not be essential for the qualitative studies in this section. For the application to ep scattering in the next section, where we will compare our results with data from HERA, we will perform our calculations in the hadronic rest system, which in that case should be more accurate.

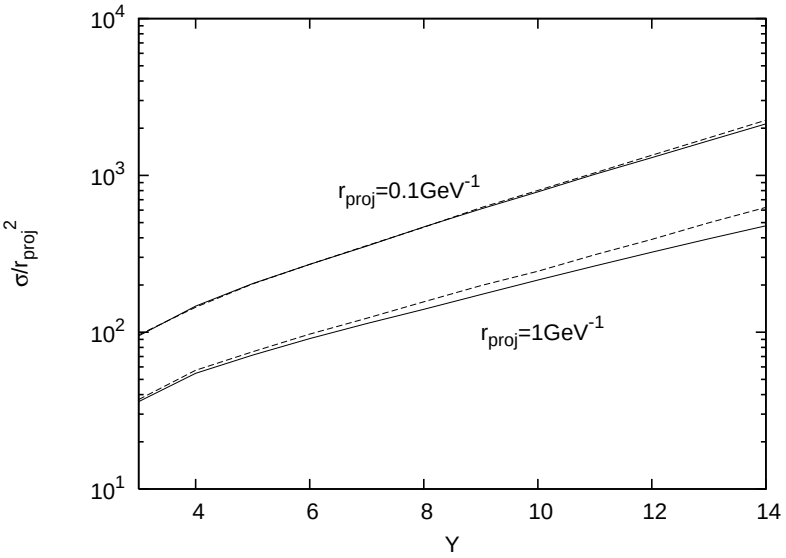

Figure 16: The dipole–nucleus cross section for $r_{\rm proj} = 0.1$ and 1 GeV^{-1} and $A = 200$. The unitarised result is shown by the solid lines, and the one-pomeron contribution by the dashed lines.

The results for $A = 200$ and $r_{\rm proj} = 0.1$ and 1 GeV^{-1} are shown in figure 16. Results are presented both for single pomeron exchange and including unitarisation. The effect of unitarisation grows with nuclear size and with the size of the projectile. For a small projectile of size 0.1 GeV^{-1} we can see the effect of colour transparency, as the cross sections for the unitarised and the one pomeron calculations are almost identical. For a larger projectile we do see a clear effect from unitarisation, but even for $r_{\rm proj} = 1$ GeV^{-1} and a nucleus with $A = 200$ this effect is only about 20 percent in the rapidity interval $10 - 14$. For smaller nuclei the effect will be correspondingly smaller.

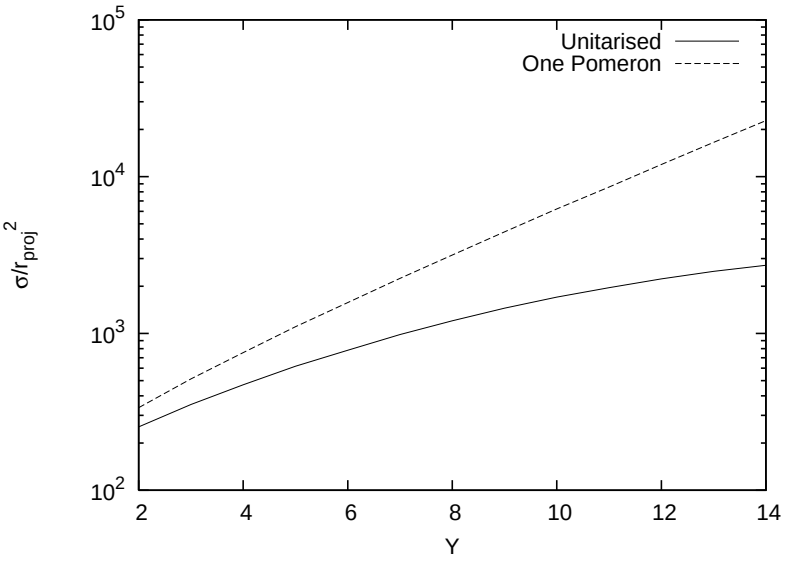

Figure 17: The scaled dipole–nucleus cross section, *without* conservation of energy, for A = 200 with a projectile of size 1 GeV^{-1}. The full and dashed line shows the result with and without unitarisation respectively.

It is also interesting to study our toy model without energy conservation, and figure 17 shows results for $r_{\mathrm{proj}} = 1\ \mathrm{GeV}^{-1}$ and $A = 200$, corresponding to the larger projectile in figure 16. The result is qualitatively similar to the corresponding results for dipole–dipole collisions, in the sense that the one-pomeron result is a straight line, while with unitarisation the suppression is increasing for larger Y-values, and the curve bends downwards. However, as expected the unitarisation effect is here quantitatively much larger.

Comparing the results in figures 16 and 17 we see that including energy conservation very strongly reduces the cross section. This suppression becomes larger for higher energies, which gives an effective slope, λ_{eff}, which decreases with energy in a way characteristic for saturation. The reduction of the gluon density due to energy conservation is also so large that the unitarity effects become comparatively small for available energies, even for large nuclei.

6.4 F_2 at HERA

When we apply our model to deep inelastic ep scattering we want to emphasize that we here only want to study the qualitative behavior. We postpone a quantitative comparison with HERA data to a future publication, where we can include effects of colour recombination and improve the simple toy model for the proton target.

For the application to DIS ep collisions we here use the same toy model described in section 6.3, with $A = 1$. We also identify Q^2 directly with $4/r_{\mathrm{proj}}^2$ without taking into account the detailed effects of the photon wavefunction. This implies that the number of dipoles in the target is much smaller than the number of dipoles in an onium state developed to large Y-values as described in section 6.1. Hence, the collision is more similar to the symmetric onium–onium scattering than to the very unsymmetric onium–nucleus collision.

To reduce the frame dependent effects discussed in section 4.4, we therefore study the dipole–proton collisions in the overall rest frame. We neglect possible correlations between the target dipoles, which thus are assumed to evolve independently. As the unitarisation effects turn out to be small, and we here only study the total cross section, it is also possible to neglect the fluctuations in the number of primary target dipoles.

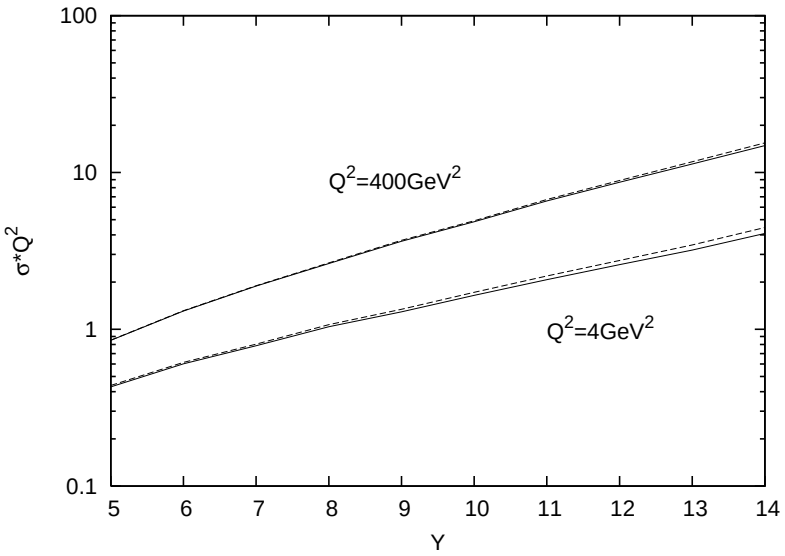

Figure 18: The scaled dipole–p cross section as a function of $\log 1/x$, for $Q^2 = 4$ GeV^2 and $Q^2 = 400$ GeV^2. The unitarised results are shown by the solid lines while the dashed lines show the one-pomeron results.

The resulting dipole–nucleon cross section is shown in figure 18 for two different projectile sizes, corresponding to $Q^2 = 4\,\mathrm{GeV}^2$ and $Q^2 = 400\,\mathrm{GeV}^2$. In this figure we also show the result for single pomeron exchange, i.e. without unitarisation corrections, and we here see that the effect from unitarisation is quite small.

Fig. 19 shows the corresponding results without energy conservation. (The results presented here are obtained for the cutoff $\rho = 0.02$ GeV^{-1}, and therefore somewhat lower than the limiting values for $\rho \to 0$.) We see that without unitarisation and without energy conservation, the cross section grows exponentially with $Y = \log 1/x$, or as a power of x. With unitarisation (but without energy conservation) the growth rate is, as expected, reduced and becomes continuously smaller with decreasing x. We note, however, that energy conservation has a similar effect, also without unitarisation, and the reduction in the cross section due to energy conservation is so large that including unitarisation does not have a significant effect.

In figure 18 we also see that the logarithmic slope $\lambda_{\mathrm{eff}} = d(\log\sigma)/d(\log 1/x)$ is increasing with increasing Q^2. As discussed above, λ_{eff} is not a constant for fixed Q^2, but depends on both Q^2 and x, when unitarisation and/or energy conservation is taken into account. To compare with experimental data we show in figure 20 λ_{eff} determined in the x-interval used in the analysis by H1 [21], which varies from $x \approx 2 \times 10^{-5}$ for $Q^2 = 1.5$ GeV^2 to $x \approx 3 \times 10^{-2}$ for $Q^2 = 90$ GeV^2. We note that the result of our crude model is not far

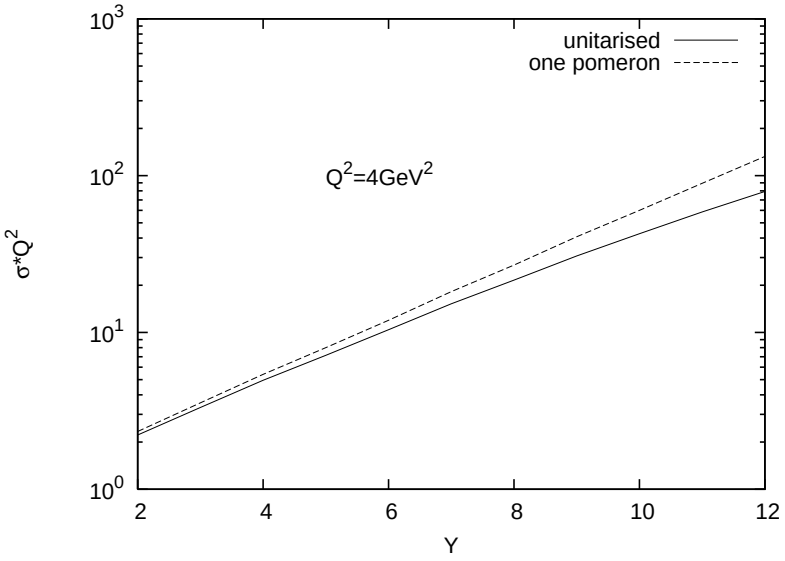

Figure 19: The scaled dipole–p cross section as a function of $\log 1/x$ calculated *without* energy conservation using $\rho = 0.02$ GeV^{-1}. Both the unitarised (full line) and the one-pomeron (dashed line) calculations are shown.

from the experimental data, although the dependence on Q^2 is somewhat weaker in the model calculations. As in figure 18 we see that the effect of unitarisation is small, and, as expected, it gets further reduced for larger Q^2-values. From figure 19 we see that the result without energy conservation and unitarisation corresponds to a much larger effective slope, and also including unitarisation the result for λ_{eff} is roughly a factor two larger than the corresponding result in figure 18.

In conclusion we find that the result of our simple model is surprisingly close to experimental data from HERA. This is very encouraging, especially since we have not attempted to tune the model in any way. The effect of energy conservation is a suppression for small x-values and small Q^2, which is qualitatively similar to the effect expected from unitarisation. This suppression is so strong that the effect from adding unitarisation is only a very small correction, visible for small Q^2-values.

7. Conclusions

Including both higher-order corrections and unitarisation effects in the high-energy limit of QCD is not a simple task. Unitarisation effects are more easily included in a dipole picture formulation in transverse coordinate space, while higher-order corrections are more easily formulated in transverse momentum space. In this report we have used as a starting point that a large part of the NLO corrections to BFKL are due to effects of energy-momentum conservation, which again are more easily formulated in transverse momentum space. However, after noting similarities between the LDC and Mueller dipole formulations of high energy QCD, we conjecture that also in the latter case, the essential contribution

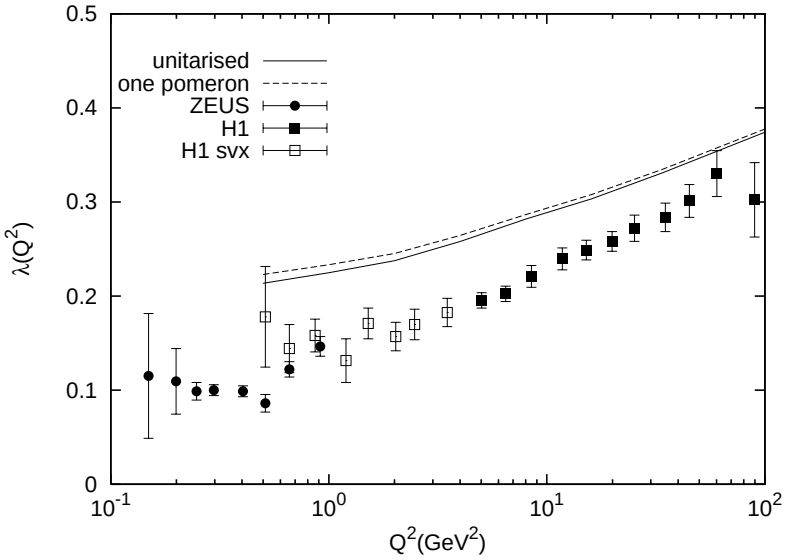

Figure 20: The effective slope measured at different Q^2 compared to data from HERA. The full line is our model including unitarisation, while the dashed line is without. Filled circles are data from ZEUS [45], filled [46] and open [22] squares are data from H1.

to the cross section comes from a subset of dipoles between real final-state gluons, which necessarily must respect energy and momentum conservation.

We have presented a way to implement energy and momentum conservation in the Mueller dipole model. This is a necessary, although not sufficient, requirement for selecting only final-state gluons, and should also include most NLO corrections to the BFKL evolution. Our way to implement energy-momentum conservation also eliminates the need for a cutoff for small dipoles in Mueller's formalism, in which the large number of small dipoles causes problems for a numerical treatment. Thus the number of dipoles produced in the evolution is drastically reduced. This applies not only to the number of very small dipoles, which do not much affect the resulting cross sections. Also the number of large dipoles is reduced, resulting in a drastic reduction of the cross section and in the effective slope $\lambda_{\text{eff}} = d\log F_2/d\log x$.

Also in standard BFKL evolution one would expect a large reduction of the effective slope due to unitarisation effects. In our case the growth of the cross section is already damped, making the inclusion of unitarisation a rather small effect for the total cross section, even for deeply inelastic virtual photon scattering on large nuclei.

Comparing with the results of [20], we find a larger effect from energy-momentum conservation. One reason seems to be the inclusion of p_--conservation, which in our formalism is found to have an important effect. Thus we find that including only conservation of p_+, and not of p_-, increases the cross section by a factor 2 (3) for dipole–proton collisions at $Q^2 = 4$ (400)GeV^2. Conservation of p_- is related to the so called consistency constraint [47], and in [20] this contribution to the NLO BFKL kernel is neglected, with the motivation that saturation effects suppress the gluon density so that this contribution is less important. Naturally, what is physically relevant is only the combined effect of both

energy conservation and saturation. Including the contributions in different order, will also give different weights to the two effects. We feel that energy and momentum conservation is the more fundamental phenomenon, and hence obtain a much smaller effect from saturation.

To investigate the scattering on nuclei we have introduced a toy model, where the nucleons are treated as a collection of dipoles with a Gaussian distribution in sizes and impact parameter. We also use this to model the scattering on a single nucleon and compared our results with HERA data. Although we made no tuning of the parameters of our model, we obtain a good semi-quantitative description of the effective slope, λ_{eff}, measured at low x and Q^2 at HERA.

Thus encouraged we will now continue to develop our model, and there are several things which we would like to improve. A major development would be to achieve a formalism which is completely frame independent. This would entail the inclusion of true gluon recombinations in the dipole evolution, and also a better understanding of the "effective" gluons with small transverse separation described in section 4.3. In this way we hope to also be able to use our formalism to describe exclusive final-state properties. Another important development would be to include effects of a running α_s, and also to improve our nucleon toy model to investigate the impact of our formalism in nucleus–nucleus collisions. We intend to return to all these issues in forthcoming publications.

References

[1] E. A. Kuraev, L. N. Lipatov, and V. S. Fadin *Sov. Phys. JETP* **45** (1977) 199–204.

[2] I. I. Balitsky and L. N. Lipatov *Sov. J. Nucl. Phys.* **28** (1978) 822–829.

[3] L. V. Gribov, E. M. Levin, and M. G. Ryskin *Phys. Rept.* **100** (1983) 1–150.

[4] K. Golec-Biernat and M. Wusthoff *Phys. Rev.* **D59** (1999) 014017, hep-ph/9807513.

[5] J. R. Forshaw, G. Kerley, and G. Shaw *Phys. Rev.* **D60** (1999) 074012, hep-ph/9903341.

[6] J. Bartels, K. Golec-Biernat, and H. Kowalski *Phys. Rev.* **D66** (2002) 014001, hep-ph/0203258.

[7] A. H. Mueller *Nucl. Phys.* **B415** (1994) 373–385.

[8] A. H. Mueller and B. Patel *Nucl. Phys.* **B425** (1994) 471–488, hep-ph/9403256.

[9] A. H. Mueller *Nucl. Phys.* **B437** (1995) 107–126, hep-ph/9408245.

[10] I. Balitsky *Nucl. Phys.* **B463** (1996) 99–160, hep-ph/9509348.

[11] Y. V. Kovchegov *Phys. Rev.* **D60** (1999) 034008, hep-ph/9901281.

[12] E. Iancu, A. Leonidov, and L. D. McLerran *Nucl. Phys.* **A692** (2001) 583–645, hep-ph/0011241.

[13] E. Ferreiro, E. Iancu, A. Leonidov, and L. McLerran *Nucl. Phys.* **A703** (2002) 489–538, hep-ph/0109115.

[14] V. S. Fadin and L. N. Lipatov *Phys. Lett.* **B429** (1998) 127–134, hep-ph/9802290.

[15] M. Ciafaloni and G. Camici *Phys. Lett.* **B430** (1998) 349–354, hep-ph/9803389.

[16] G. P. Salam *Acta Phys. Polon.* **B30** (1999) 3679–3705, hep-ph/9910492.

[17] J. R. Andersen and W. J. Stirling *JHEP* **02** (2003) 018, hep-ph/0301081.

[18] L. H. Orr and W. J. Stirling *Phys. Rev.* **D56** (1997) 5875–5884, hep-ph/9706529.

[19] E. Levin and K. Tuchin *Nucl. Phys.* **B573** (2000) 833–852, hep-ph/9908317.

[20] E. Gotsman, E. Levin, U. Maor, and E. Naftali hep-ph/0504040.

[21] **H1** Collaboration, C. Adloff *et al. Phys. Lett.* **B520** (2001) 183–190, hep-ex/0108035.

[22] A. Petrukhin, "New Measurement of the Structure Function $F_2(x, Q^2)$ at low Q^2 with Initial State Radiation Data." Proceedings of DIS04, Štrbské Pleso, Slovakia, 2004.

[23] E. Iancu, K. Itakura, and S. Munier *Phys. Lett.* **B590** (2004) 199–208, hep-ph/0310338.

[24] M. Ciafaloni, D. Colferai, and G. P. Salam *Phys. Rev.* **D60** (1999) 114036, hep-ph/9905566.

[25] G. Gustafson *Phys. Lett.* **B175** (1986) 453.

[26] G. Gustafson and U. Pettersson *Nucl. Phys.* **B306** (1988) 746.

[27] L. Lönnblad *Comput. Phys. Commun.* **71** (1992) 15–31.

[28] K. Hamacher and M. Weierstall hep-ex/9511011.

[29] N. Brook, R. G. Waugh, T. Carli, R. Mohr, and M. Sutton. Prepared for Workshop on Future Physics at HERA (Preceded by meetings 25-26 Sep 1995 and 7-9 Feb 1996 at DESY), Hamburg, Germany, 30-31 May 1996.

[30] G. P. Salam *Comput. Phys. Commun.* **105** (1997) 62–76, hep-ph/9601220.

[31] A. H. Mueller and G. P. Salam *Nucl. Phys.* **B475** (1996) 293–320, hep-ph/9605302.

[32] G. P. Salam *Nucl. Phys.* **B461** (1996) 512–538, hep-ph/9509353.

[33] B. Andersson, G. Gustafson, and J. Samuelsson *Nucl. Phys.* **B467** (1996) 443–478.

[34] B. Andersson, G. Gustafson, and H. Kharraziha *Phys. Rev.* **D57** (1998) 5543–5554, hep-ph/9711403.

[35] S. Catani, F. Fiorani, and G. Marchesini *Phys. Lett.* **B234** (1990) 339.

[36] M. Ciafaloni *Nucl. Phys.* **B296** (1988) 49.

[37] G. Altarelli and G. Parisi *Nucl. Phys.* **B126** (1977) 298.

[38] V. N. Gribov and L. N. Lipatov *Yad. Fiz.* **15** (1972) 781–807.

[39] L. N. Lipatov *Sov. J. Nucl. Phys.* **20** (1975) 94–102.

[40] Y. L. Dokshitzer *Sov. Phys. JETP* **46** (1977) 641–653.

[41] H. Kharraziha and L. Lönnblad *JHEP* **03** (1998) 006, hep-ph/9709424.

[42] B. Andersson, G. Gustafson, L. Lönnblad, and U. Pettersson *Z. Phys.* **C43** (1989) 625.

[43] **Small x** Collaboration, B. Andersson *et al. Eur. Phys. J.* **C25** (2002) 77–101, hep-ph/0204115.

[44] G. P. Salam *JHEP* **03** (1999) 009, hep-ph/9902324.

[45] **ZEUS** Collaboration, J. Breitweg *et al. Phys. Lett.* **B487** (2000) 53–73, hep-ex/0005018.

[46] **H1** Collaboration, C. Adloff *et al. Eur. Phys. J.* **C21** (2001) 33–61, hep-ex/0012053.

[47] J. Kwiecinski, A. D. Martin, and P. J. Sutton *Z. Phys.* **C71** (1996) 585–594, hep-ph/9602320.